Super-K,K2K,JHFnu and UNO: Past,Present and Future

Chiaki Yanagisawa[*][†]

Department of Physics and Astronomy, Stony Brook University, Stony Brook, NY 11794-3800, U.S.A.
E-mail: `chiaki@nngroup.physics.sunysb.edu`

ABSTRACT: This article is based on the talk give at the conference, and review the latest results from Super-Kamiokande-I (SK-I) and K2K-I; the status of Super-Kamiokande-II (SK-II) and K2K-II; and prospects for the two future experiments, JHFnu and UNO.

1. Super-Kamiokande-I

Super-Kamiokande before the unfortunate accident in 2001 is now officially called Super-Kamiokande-I. In this section, three topics, atmospheric neutrino oscillation, solar neutrino oscillation and nucleon decay search, will be covered.

1.1 Atmospheric neutrino oscillation

Latest changes in the Monte Carlo (MC) generator, reconstruction programs, data reduction processes, atmospheric neutrino fluxes, and calibration for water transparency and for the outer detector resulted in noticeable changes in oscillation analyses. For the current data analyses the atmospheric neutrino fluxes used are based on the 2001 3-D calculation by Honda *et.al.* [1], resulting in reduced total fluxes and enhancement of the flux at low energies and near the horizon. However, as the leptons produced by low energy neutrinos have smaller energies, the neutrino direction is smeared and these differences do not affect much except for the normalization. In this section results using the data accumulated in the period from April 1996 to July 2001, corresponding to 1489 live-days are presented.

Figure 1 shows the zenith angle distributions of various event classes: *e*-like, μ-like, sub-GeV, multi-GeV, single ring, multi-ring, fully contained (FC), partially contained (PC), and upward-going muons. For events in multi-ring class, only those events where the most energetic ring is μ-like are included. The data are represented by solid circles while Monte

---

[*]Speaker.

[†]For the Super-K,K2K,JHFnu and UNO collaborations.
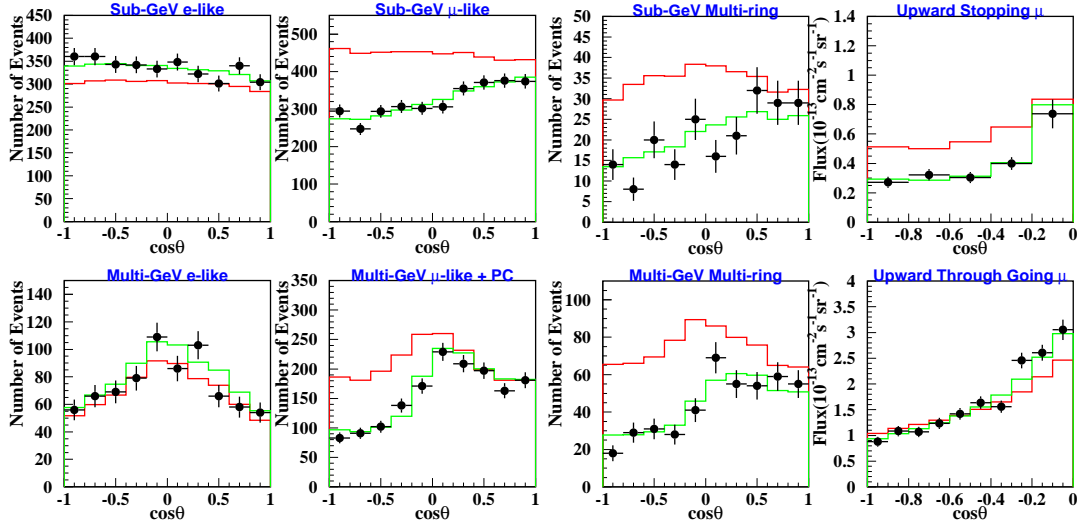
Figure 1: Zenith angle distributions of single ring atmospheric neutrinos events.
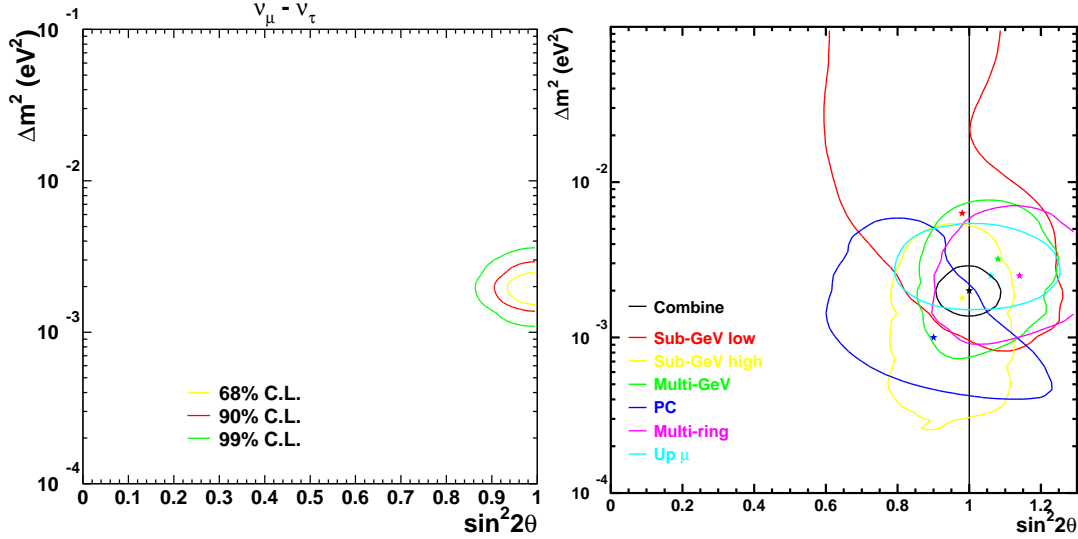
Figure 2: Allowed regions of oscillation parameters at 68, 90 and 95% C.L. (left). 90% C.L. allowed regions of oscillation parameters using events from each class (right).

Carlo (MC) predictions with and without oscillation effect are shown by light(green) and dark(red) dashed line histograms. The MC predictions with the oscillation effect are with the best fitted parameters. Note that no enhancement is seen from the 3-D calculation for the neutrinos coming from the horizon for the reason described above.

Combining the events from all the classes, as summarized in Figure 2 (left), the best fit result on the oscillation parameters are found to be: $\Delta m^2 = 2.0 \times 10^{-3} eV^2$ and $sin^2 2\theta = 1.0$ with $\chi^2_{min} = 170.8/170$ d.o.f. For the null oscillation hypothesis, $\chi^2_{min} = 445.2/172$ d.o.f. This best value for Δm^2 is somewhat different from the previous result of $\Delta m^2 = 2.5 \times$
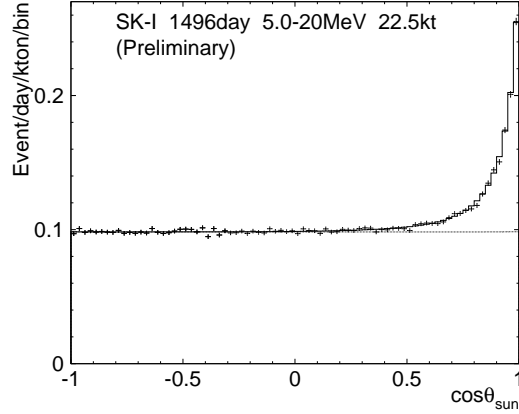
Figure 3: Distribution of $\cos\theta_{Sun}$ of the solar neutrino event candidates.

$10^{-3}eV^2$. Close inspections of individual effects due to modifications since the previous result reveal that each modification contributes to a shift in the allowed region of the oscillation parameters, however small it may be, and that these contributions add up to the final difference. Analyses using events from each class at a time produce consistent results as shown in Figure 2 (right). This observation assures us that the latest result is quite reasonable.

1.2 Solar neutrino oscillation

In this section, solar neutrino results using the data accumulated in the period from May 1996 to July 2001, corresponding to 1496 live-days, are presented. Figure 3 is the distribution of cosine of the angle of the recoil electron with respect to the direction from the Sun for the solar neutrino event candidates. Clearly seen is the peak toward $\cos\theta_{Sun} = 1$, which indicate solar neutrino events are detected. After the background subtraction, the number of solar neutrino events observed is found to be $22,400 \pm 230$ corresponding to an event rate of 14.5 events/day. This observed number of events is translated into the ^8B neutrino flux of $2.35 \pm 0.02 \pm 0.08 \times 10^6/cm^2/sec$. If the flux is normalized to the 2001 flux calculation by Bahcal, Pensonneault, and Basu [2] ($5.50 \times 10^6/cm^2/sec$), the ratio is $0.465 \pm 0.005^{+0.016}_{-0.015}$. The high statistics of the SK-I solar neutrino data (a mixture of charged current CC and neutral current NC events) together with the SNO CC and NC event data [3] makes it possible to measure the total solar neutrino flux. The solar neutrino flux measured by SK-I using elastic scattering events ϕ_{ES} is a sum of the flux of the ν_e and 15% of the flux of $\nu_{\mu,\tau}$ due to the NC event contribution, *i.e.*, $\phi_{ES} = \phi_e + 0.15\phi_{\nu_\mu + \nu_\tau}$. SNO can measure the ϕ_{CC} using ν_e CC events, and the ϕ_{NC} using $\nu_{e,\mu,\tau}$ NC events separately where $\phi_{CC} = \phi_{\nu_e}$ and $\phi_{NC} = \phi_{\nu_e} + \phi_{\nu_\mu} + \phi_{\nu_\tau}$. The result of this combined analysis is that the total measured solar flux ϕ_{exp} is 5.09 ± 0.7 which is consistent with the standard solar model prediction of $\phi_{SSM} = 5.05^{+1.01}_{-0.82}$. Figure 4 summarizes this result as allowed regions at different confidence levels in $\phi_{\nu_\mu + \nu_\tau}$ vs. ϕ_{ν_e} space. Note that the SSM flux prediction is shown as straight lines.
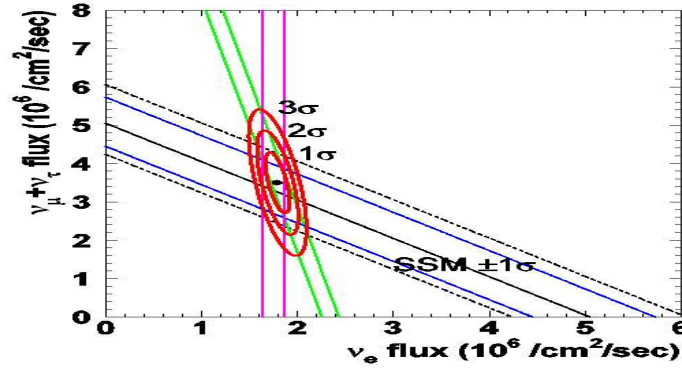
Figure 4: Measurements of $\phi_{\nu_\mu + \nu_\tau}$ vs. ϕ_{ν_e} using the SK-I and SNO data.
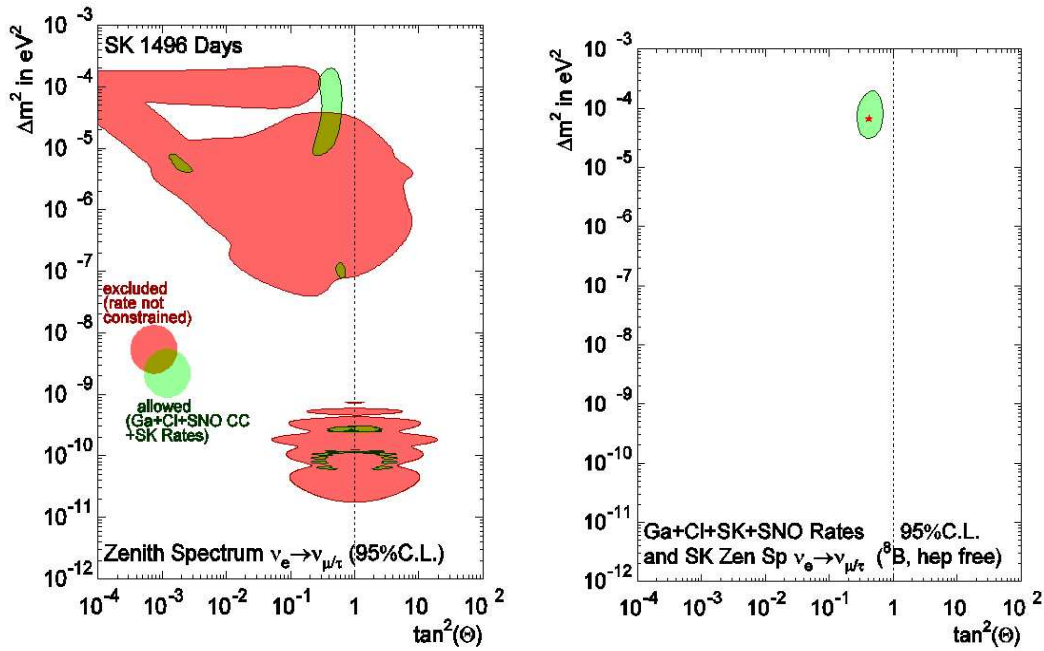
Figure 5: Left: 95% C.L. excluded region using the SK-I spectrum information in different zenith angle regions together with the 95% allowed region using all the measured solar neutrino event rates from all the solar neutrino experiments. Right: 95% C.L. allowed region using the SK-I spectrum information in different zenith angle regions together with all the measured solar neutrino event rates from all the solar neutrino experiments.

Figure 5 (left) is a summary of SK-I analysis using spectrum shape from different zenith angle regions of the solar neutrinos without the rate constraint. The lightly shaded (green) areas are the excluded regions at 95% C.L. by SK-I. In this figure, also shown are the allowed regions (medium dark shaded or pink areas) at 95% C.L. using the rate information from the gallium, chlorine, SNO (charge current) and SK-I experiments. All the solutions except for the large mixing angle MSW solution (LMA) are excluded. Even
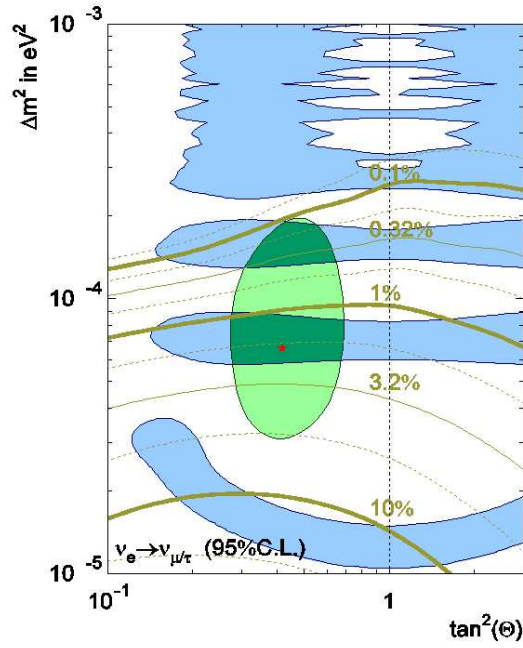
Figure 6: 95% C.L. allowed region using the results from all the solar neutrino experiments - the same as the shown in the previous figure compared with the KamLAND result.

a half of the area in the LMA solution is excluded. If all the rate measurements by all the experiments and SK-I zenith spectrum measurement are combined, the only LMA solution survives at 95% C.L. as in Figure 5 (right).

Although KamLAND is not a solar neutrino experiment, it is very interesting to compare its result with that presented in Figure 5 (right). The comparison is done in Figure 6 where a shaded ellipse (green) in the middle represents the 95% allowed region of the combined result from all the solar neutrino experiments shown in Figure 6 and other shaded regions are the allowed regions at 95% C.L. from KamLAND. In addition, the lines with percentage (green-brown) show the expected oscillation parameter values for given values at SK-I for the day/night asymmetry defined by $\frac{(D-N)}{(D+N)/2}$ with D(N) for the number of events in daytime (nighttime). High statistics experiments such as SK-I, SK-II, and UNO can still play an important role to narrow down possible values for the oscillation parameters using this asymmetry.

1.3 Nucleon decays

As most of Grand Unified Theories predict nucleon decays, an observation or even a hint of such decays could be the next big thing that would give another crack in the Standard Model after the discovery of neutrino oscillations in atmospheric and solar neutrinos. SK-I was the only experiment that could set the better limits on the nucleon stability than IMB-3 until SK-II accumulates more statistics. Figure 7 summarizes the status of upper limits on nucleon partial lifetimes measured by SK-I together with the results from IMB3,

Summary of Nucleon Decay Searches

mode	exposure (kt·yr)	εB_m (%)	observed event	B.G.	τ/B limit (10^{32} yrs)
$p \to e^+ + \pi^0$	92	40	0	0.2	54
$p \to \mu^+ + \pi^0$	92	32	0	0.2	43
$p \to e^+ + \eta$	92	17	0	0.2	23
$p \to \mu^+ + \eta$	92	9	0	0.2	13
$n \to \bar{\nu} + \eta$	45	21	5	9	5.6
$p \to e^+ + \rho$	92	4.2	0	0.4	5.6
$p \to e^+ + \omega$	92	2.9	0	0.5	3.8
$p \to e^+ + \gamma$	92	73	0	0.1	98
$p \to \mu^+ + \gamma$	92	61	0	0.2	82
$p \to \bar{\nu} + K^+$	92				22
$\quad K^+ \to \nu\mu^+$ (spectrum)		34	–	–	3.8
$\quad$ prompt $\gamma + \mu^+$		8.6	0	0.7	11
$\quad K^+ \to \pi^+\pi^0$		6.0	0	0.6	7.9
$n \to \bar{\nu} + K^0$	92				2.0
$\quad K^0 \to \pi^0\pi^0$		6.9	14	19.2	3.0
$\quad K^0 \to \pi^+\pi^-$		5.5	20	11.2	0.8
$p \to e^+ + K^0$	92				10.7
$\quad K^0 \to \pi^0\pi^0$		9.2	1	1.1	8.7
$\quad K^0 \to \pi^+\pi^-$					
$\qquad$ 2-ring		7.9	5	3.6	4.0
$\qquad$ 3-ring		1.3	0	0.1	1.7
$p \to \mu^+ + K^0$	92				13.9
$\quad K^0 \to \pi^0\pi^0$		5.4	0	0.4	7.1
$\quad K^0 \to \pi^+\pi^-$					
$\qquad$ 2-ring		7.0	3	3.2	4.9
$\qquad$ 3-ring		2.8	0	0.3	3.7

Figure 7: A summary of nucleon decay partial lifetimes by SK-I/Kamiokande/IMB 3.

Kamiokande (KAM) and Soudan 2. As you can see, improvements of a factor of 2-10 have been achieved by SK-I over the IMB3 result which was the best before the SK-I result. However, SK-I has not found any sign of nucleon stability yet.

1.4 SK-II

In December 2002, SK-II started to take data 13 months after the accident. Although for SK-II the photomultiplier (PMT) coverage is reduced to 47% of that for SK-I, except for low energy physics such as low energy solar neutrinos, the detector capability is not hampered by this reduction. Figure 8 (left) is the SK-II detector just before the water started to fill the tank and a typical cosmic ray event is shown in Figure 8 (right).

2. K2K

2.1 K2K-I/K2K-II experiments

Because of the accident in SK, K2K was forced to stop the data taking in 2001-2002. Now K2K before the SK-I accident is called K2K-I and the current experiment is K2K-II. Figure 9 is the K2K-I near detector complex consisting of an 1kton water Cherenkov detector (1kt), a scifi/water target tracker (Scifi), a lead glass calorimeter (LG), and a muon range detector (MRD). During the shutdown of 2002-2003, LG was removed and a new tracker/calorimeter (SciBar) was installed. This detector is made of scintillator
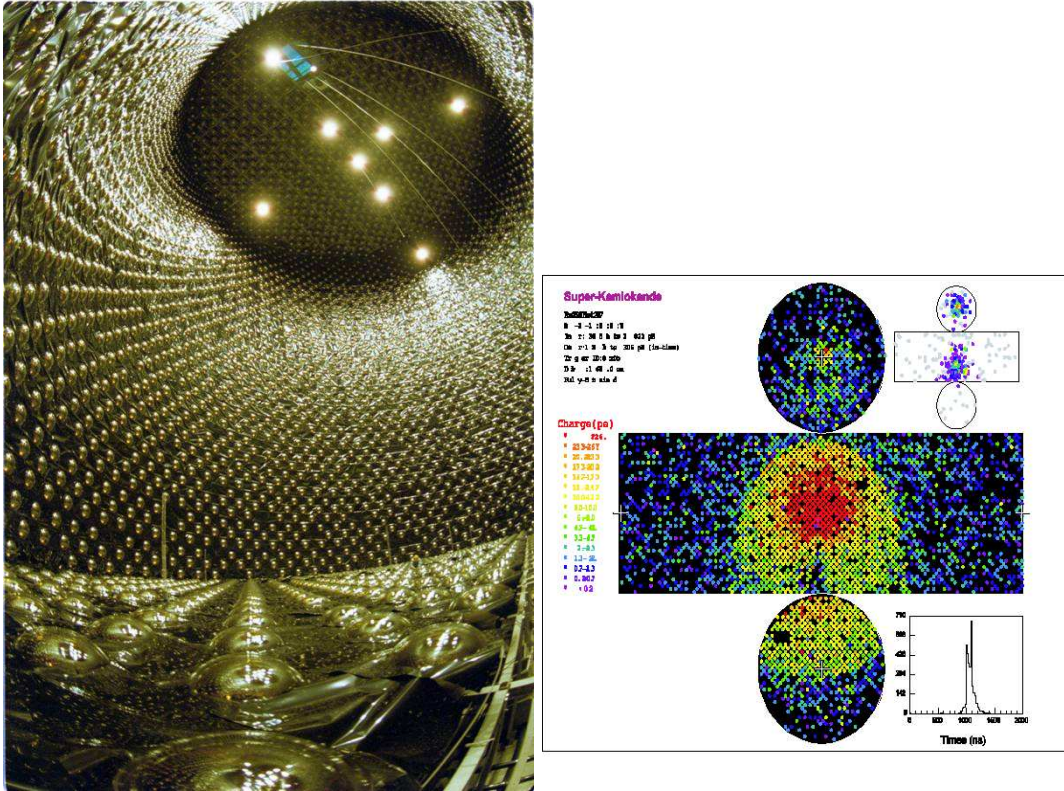
Figure 8: Left: SK-II detector with about a half SK-I photomultiplier density. Right: A cosmic ray event detected by the SK-II detector.

bars whose signals are read by multi-anode phototubes (MPT) through wavelength-shifted scintillating fibers.

Figure 10 is a summary of the total integrated number of protons on target (pot) in units of 10^{12} together with the number of protons per pulse in units of 10^{18} as a function of time. During the entire K2K-I run period from June 1999 to July 2001, the total of 4.8×10^{19} pot were delivered. As the current plan is to accumulate the total of 1×10^{20} pot, K2K-I accumulated about a half of the total integrated neutrino flux to be delivered. K2K-II started to take data in January 2003 with SK-II as the far detector.

2.2 Neutrino energy spectrum measurement

The neutrino energy spectrum is measured by three near detector components, namely, the 1kt and the Scifi plus MRD (Fine Grained Detector-FGD). The measured neutrino energy is divided into eight bins as shown in Figure 11 (left). In this figure, the solid points with error bars are the measurements by the near detector corrected by the Monte Carlo calculation while the histogram presents the expected spectrum by Monte Carlo calculation only. For the measured points, the some parameters in Monte Carlo calculation were modified so that the difference between the measurement and the prediction gives the smallest χ^2. These parameters include re-weighting factors for each energy bin and the ratio, quasi-elastic
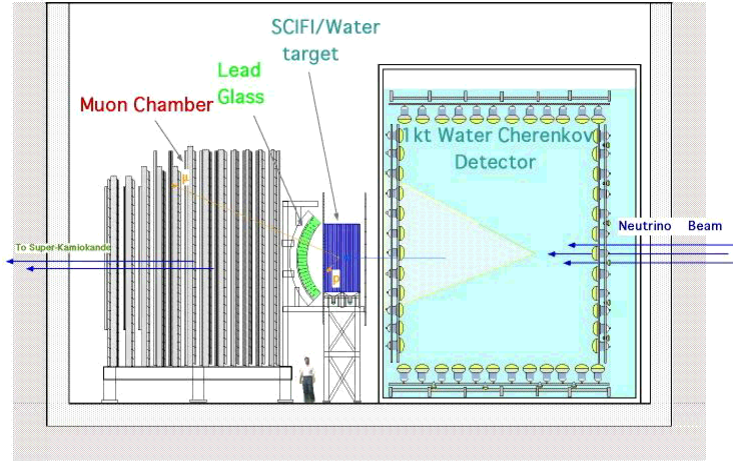
Figure 9: K2K-I detector.
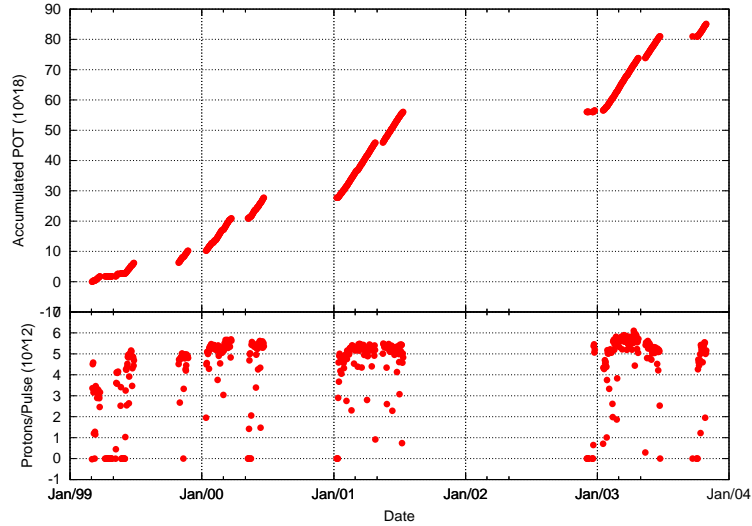
Figure 10: History of the integrated number of protons on target delivered and proton intensity as a function of time for K2K-I and K2K-II.

to non-quasi-elastic cross section. The fit result on parameter changes is summarized in Figure 11 (right).

2.3 Expected neutrino energy spectrum at SK-I

As the neutrinos are produced in the decay tunnel, we cannot consider the neutrino beam to come from a point source. Because of this, the neutrino spectra at the near detector and at SK-I are different. Therefore, it is very important to estimate the expected difference in the neutrino energy spectrum in order to extract the neutrino oscillation information. K2K-I estimates the ratio of the fluxes for a given energy bin, at the near detector to at
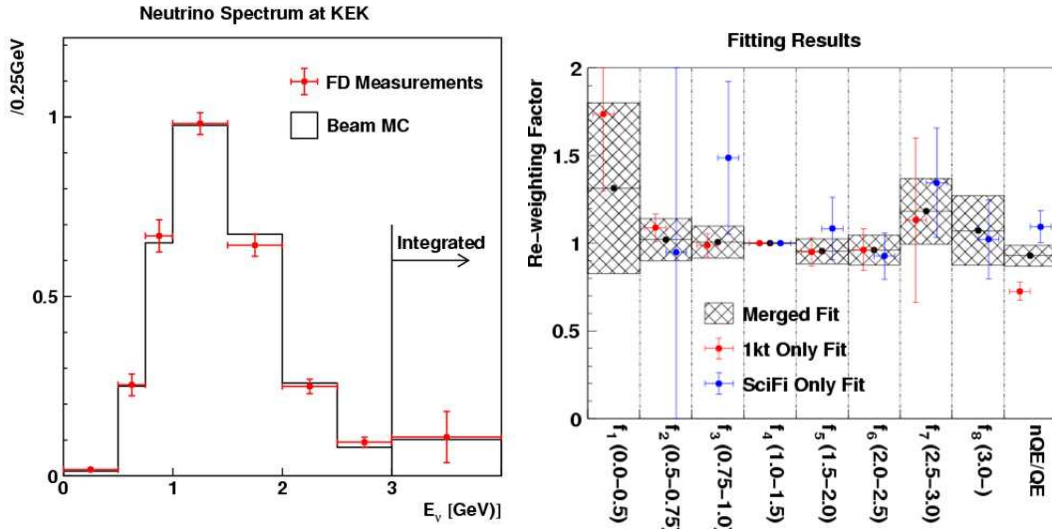
Figure 11: Left: Measured neutrino spectrum at the near detector. Right: Best fit weights used in the spectrum analysis.
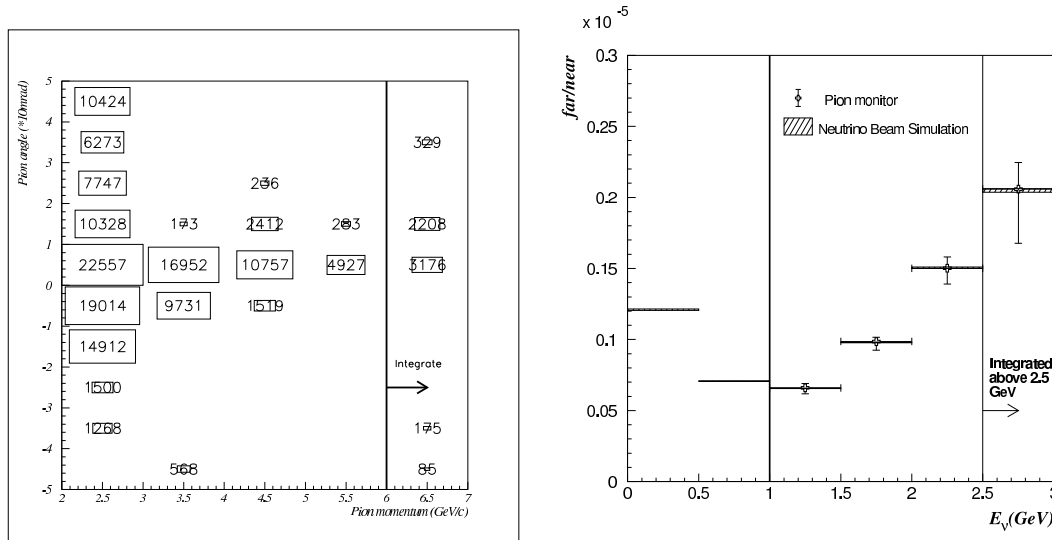
Figure 12: Left: Measured correlation between the momentum and angle of the secondary pions measured by the pion monitor right after the horns. Right: Estimated flux ratio at SK to at the near detector.

SK-I. This is done using a detailed beam Monte Carlo calculation and measurements by a pion monitor which measured the charged pion angle and momentum. The pion monitor is made of a gas Cherenkov detector and one of its measurement is shown in Figure 12
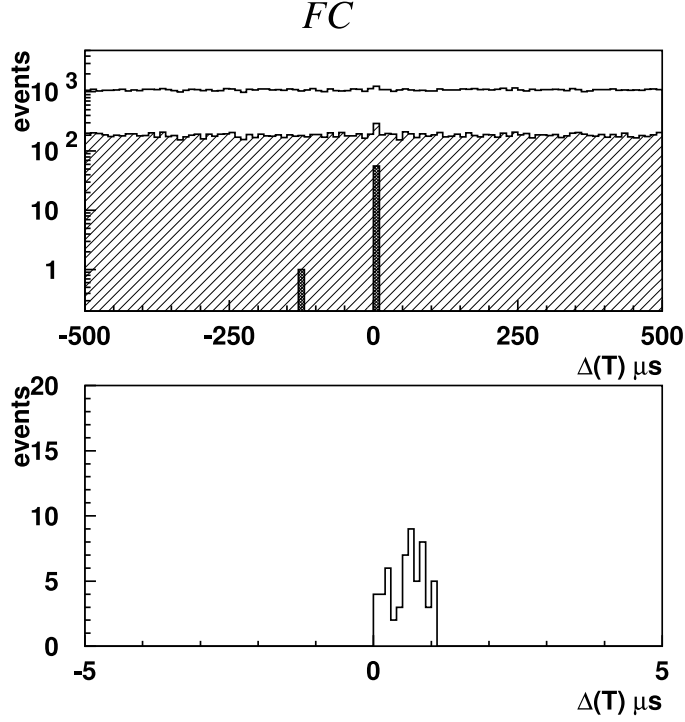
Figure 13: Timing distributions of event candidates produced by the K2K neutrino beam and detected by SK-I.

(left) where the correlation between the pion angle and momentum is given. Knowing this correlation, the beam Monte Carlo is modified to reproduce the correlation, and the expected neutrino spectra at the near detector and at SK-I is calculated by the modified Monte Carlo that uses the information from the pion monitor. Figure 12 (right) shows the expected spectrum ratios calculated by the pure beam Monte Carlo (solid line) and the modified Monet Carlo (crosses with error bars). The difference between the two results is very small. This assures us that the estimation on the ratios is very reliable.

2.4 SK-I events and oscillation analysis

Figure 13 shows the timing distribution of the events detected by SK-I after some cuts to remove most of trivial background. The upper panel is the time difference $\Delta T = T_{SK} - T_{K2K} - TOF$ between -500μs and 500μs where T_{SK}, T_{K2K}, TOF are the event time at SK-I, the corresponding neutrino beam bunch time at K2K, and the time of flight of the neutrinos from K2K to SK-I. The lower panel is the same distribution with finer binning (between -5 μs and 5 μs). Events within a 1.5 μs window are accepted as the
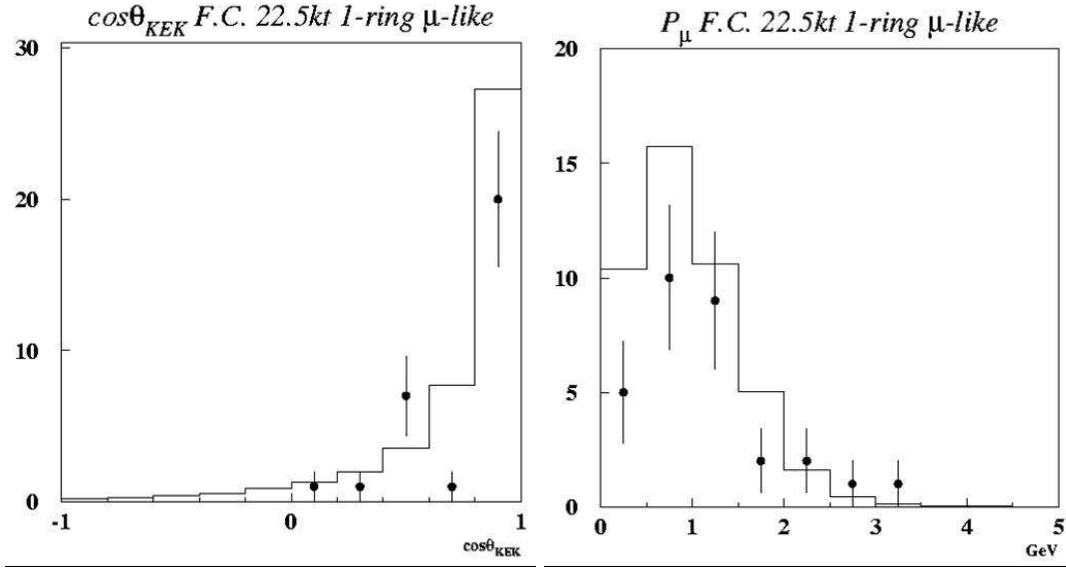
Figure 14: Left: Cosine of the muon angle measured at SK-I. Right: Muon momentum distribution at SK-I.

events produced by the K2K neutrino beam as the duration of the beam spill is 1.1 μs. In these candidate events only 10^{-3} background events are expected from the atmospheric neutrino interactions.

The numbers of events observed at SK-I in the fiducial volume of 22.5 ktons are: 30 single-ring μ-like, 2 single-ring e-like, and 24 multi-ring events, which give the total number of events of 56. The expected total number of events is $80.1^{+6.5}_{-5.4}$ in the case of no neutrino oscillation. 29 events out of 30 single-ring μ-like events are used for the spectrum analysis because the excluded event was from the run period with a different magnetic horn current from that in the rest of running period and the different neutrino energy spectra. The total observed number of events, 56, is used for the normalization.

Figure 14 shows the cosine of the muon angle with respect to the neutrino beam (left) and the muon momentum distribution (right), respectively, of single-ring μ-like events together with the Monte Carlo predictions assuming that there is no neutrino oscillation. Using these two measured quantities, K2K-I reconstructed the neutrino energy of detected single-ring μ-like neutrino events produced by the K2K beam. The reconstructed neutrino spectrum in GeV is shown in Figure 15 where the solid points with error bars represent the measured spectrum, the dashed histogram the expected distribution for the expected event rate without neutrino oscillation, the boxes the expected distribution normalized with the observed event rate for the non-oscillation case, and the histogram with thick solid line the expected spectrum using the best fit parameter values including the best oscillation parameters, $\Delta m^2 = 2.8 \times 10^{-3} eV$ and $sin^2 2\theta = 1.0$. These best fit parameters give the KS probability of 79%. In comparison to the probability of the best oscillation parameters, the probability for the non-oscillation hypothesis was found to be 0.7%, 1.3% and 16% using the rate and shape information, the rate only and the shape only, respectively. These
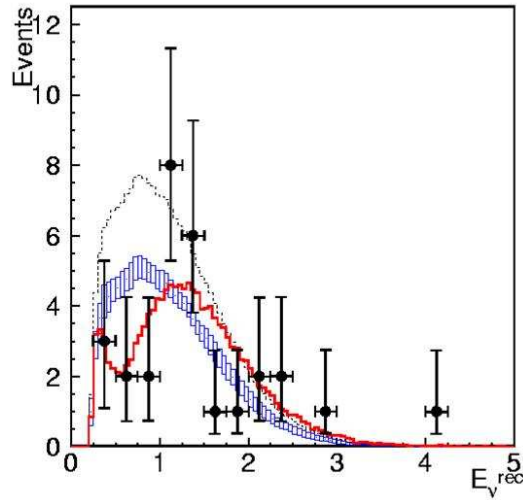
Figure 15: Measured and expected neutrino spectra at the near detector.
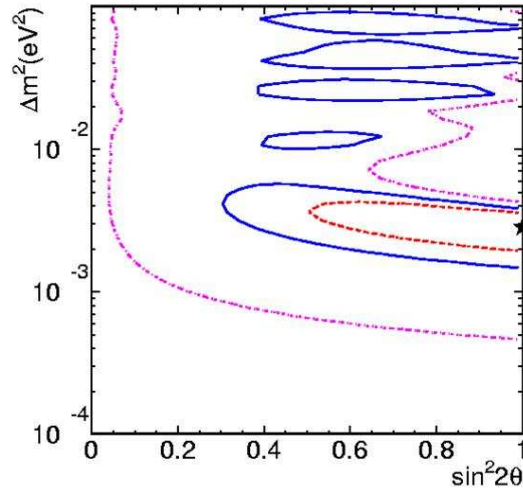
Figure 16: Allowed regions of the oscillation parameters at 68 (dark dashed or red curve), 90 (solid or blue curves) and 95% (light dashed or pink curves) C.L.

values of the probability are expected to be reduced further down to 0.08%, 0.76% and 2.9%, respectively, at the end of the K2K-II experiment. The summary of the oscillation analysis is presented in Figure 16 as allowed regions in the oscillation parameter space where 68 (dark dashed or red curves), 90 (solid or blue curves), and 95% (light dashed or pink curves) C.L. are shown.

2.5 Status of K2K-II

As mentioned earlier in this report, K2K-II has started to take data in January, 2003 with SciBar that replaced LG. The reason for this upgrade is to increase the detection efficiency
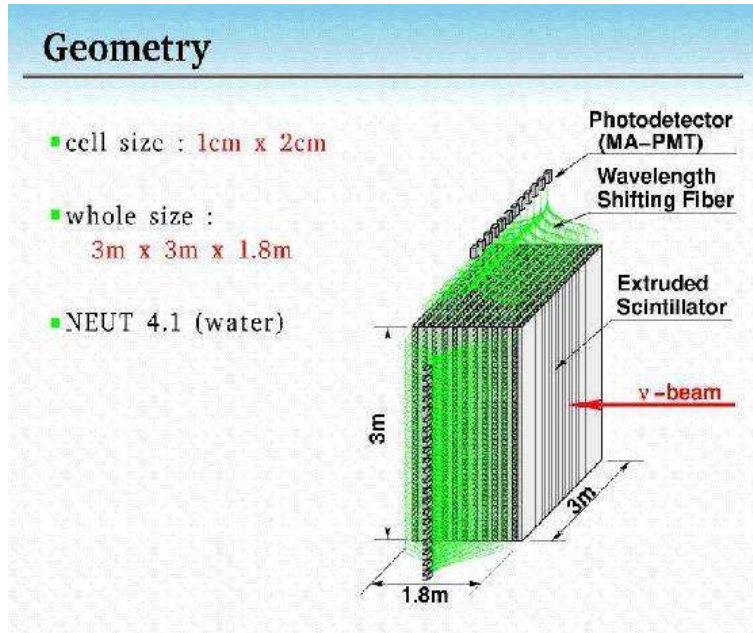
Figure 17: A sketch of SciBar with a Monte Carlo event display.

for low energy neutrinos below 1 GeV. As the deficit of events detected at SK-I is expected to be located below the neutrino energy below 1 GeV, this is very important improvement over K2K-I. The SciBar detector is made of a stack of $1.3^{cm} \times 2.5^{cm} \times 3^m$ scintillator bars, whose light output is transported by a wavelength shifter doped scintillating fiber read by a channel of MPT. Some detail of the geometry of the detector is shown in Figure 17. Major advantages of SciBar over LG are: (1) Good proton detection efficiency 70%, (2) good $p/\pi^{\pm}$ separation (the misidentification probability of $p \to \pi^{\pm}$ less than 20% for the momentum less than 1.2 GeV/c, and (3) good proton momentum resolution better than 10%. These advantages lead to a lower E_ν detection threshold.

3. JHF/J-PARC neutrino experiment JHFnu

3.1 JHF/J-PARC

An intense 50 GeV proton synchrotron is being constructed in Village of Tokai in Japan to be completed in 2007. The construction has started in 2001. This will be a multi-purpose proton beam facility. One of the use of this facility J-PARC/JHF is to build an intense neutrino beam to shoot toward SK, 295 km away to further extend the research with a long baseline neutrino oscillation experiment that has been pioneered by K2K much beyond the current K2K expectation, although at the time of this writing (early December, 2003) the approval of building the neutrino beam line is still pending but is expected be approved. The goals of this project is not only to measure more precisely Δm_{23}^2 and $sin^2 2\theta_{23}$ but also to actually observe the ν_e appearance as a result of neutrino oscillation and to measure $sin^2 2\theta_{13}$ for the first time.

Figure 18: A conceptual view of the JHFnu project.
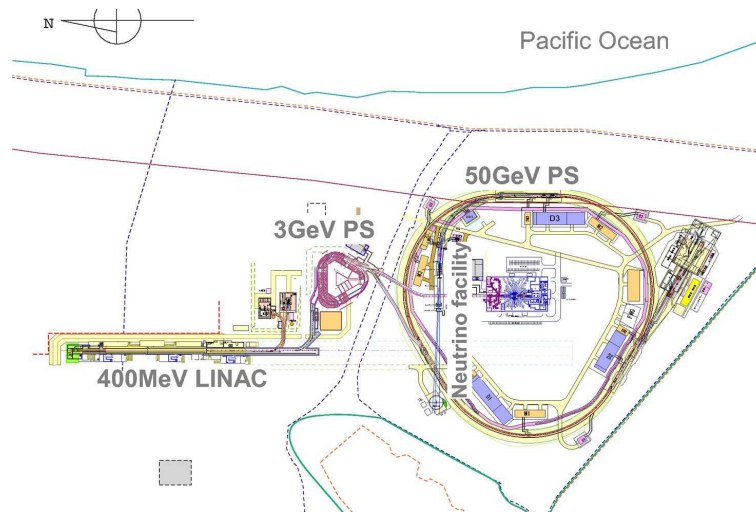
Figure 19: JHFnu accelerator complex.

Figure 18 is a sketch of JHFnu project. The intense 0.75 MW 50 GeV proton beam will generate an 8-bunch pulse over 5μs period of time every 3.94 seconds that will contain 3.3×10^{14} protons per pulse and will produce 10^{21} pot per year (130 days/year). As the second stage of the JHFnu project, it is planned to build a megaton size water Cherenkov detector called Hyper-Kamiokande near the current SK site which would be shot by even more intense neutrino beam produced by a 4 MW Super-JHF proton synchrotron. A sketch of the JHFnu facility is shown in Figure 19. A 400 MeV LINAC produce an intense proton beam which will be fed into 3 GeV PS and eventually this 3 GeV proton beam will be transfered to the 50 GeV PS. The proton beam will be then extracted and lead to a target through the transport line made of super-conducting magnets. Right after the target, the secondary beam will go through two or three magnetic horns to focus charged pions to produced an intense focused neutrino beam in a decay tunnel. The neutrino beam will be monitored and used to measure the neutrino flux and spectrum at 280 m from the target

Neutrino spectra at diff. dist

dominant syst. in K2K
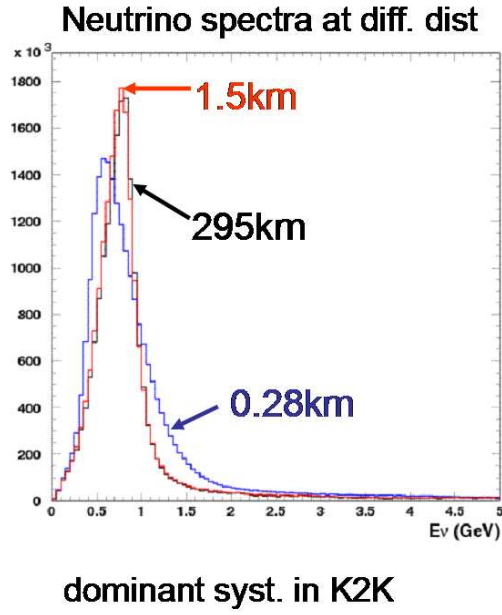
Figure 20: Expected neutrino spectra at 280 m, 1.5 km and 295 km (SK).

by a near detector complex. A possibility of building a second detector at 1.5-2.0 km from the target to measure the neutrino flux and spectrum is being discussed. At 1.5-2 km, it is expected that the neutrinos behave like being produced by a point source. In Figure 20 a comparison of the neutrino spectra at 0.28, 1.5 and 295 km is made to show that the spectrum at 1.5 km is quite similar to that at 295 km. Refer to the Letter of Intent for further detail [5].

3.2 JHFnu beam

As the Brookhaven National Laboratory proposal pointed out [4], the neutrino beam can be tuned to be narrow and its peak energy can be adjusted by a off-beam axis beam. Now that we know reasonably well where the maximum deficit of neutrino flux occurs, the neutrino beam can be optimized using this technique. Among several options, the JHFnu project plans to use $2°$ off-axis option as the first choice.

3.3 Sensitivities to Δm_{23}^2 and $sin^2 2\theta_{23}$

Figure 21 (right) shows the expected neutrino flux deficit as a function of the reconstructed neutrino energy at SK in linear (top) and log (bottom) scale. From this plot, the sensitivities can be estimated and are summarized in Figure 21 (left) where sensitivities to $sin^2 2\theta_{23}$ (top) and to Δm_{23}^2 in eV^2 (bottom) as a function of the true Δm_{23}^2 value are plotted. Here the dark solid (green) curves that have the minimum value in $0.002 < \Delta m_{23}^2 < 0.004 eV^2$ ($\delta \Delta m_{23}^2 = 1 \times 10^{-4} eV^2$, $\delta sin^2 2\theta_{23} = 0.025$) correspond to the $2°$ off-axis beam, while other curves correspond to other off-axis angles. Δm_{23}^2 and $sin^2 2\theta_{23}$ as seen in Figures.
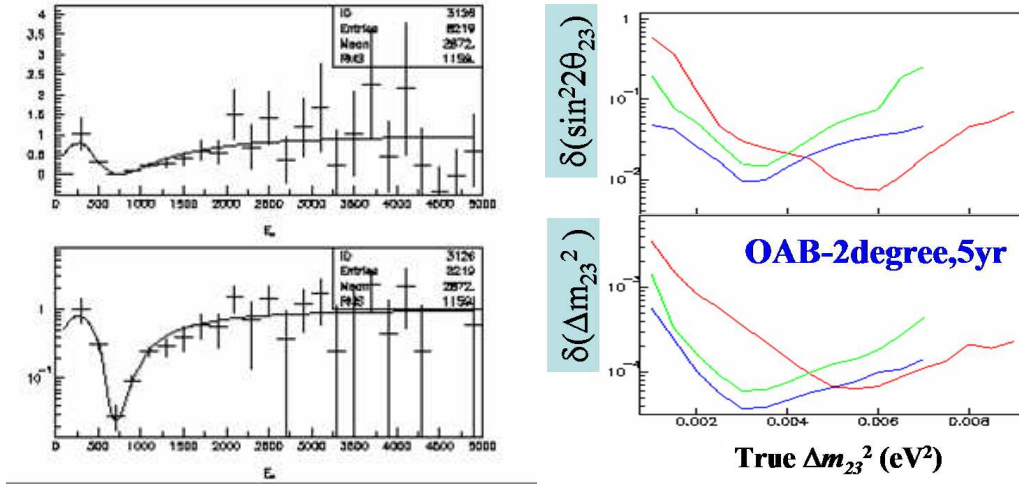
Figure 21: Left: Deficit in the neutrino flux expected at SK. Right: Sensitivities to Δm_{23}^2 and $sin^2 2\theta_{23}$.
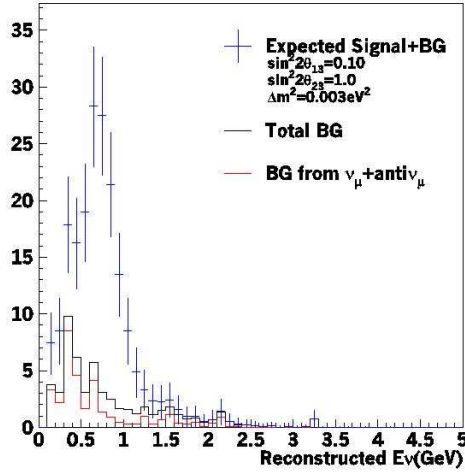
Figure 22: Distribution of reconstructed neutrino energy of ν_e events.

3.4 Sensitivity to $sin^2 2\theta_{13}$

The more ambitious goal of this project is to actually measure $sin^2 2\theta_{13}$ for the first time, although whether it can be done or not depends on how large this angle is. This measurement will have to be done by observing ν_e appearance above the expected background. Figure 22 is the reconstructed neutrino energy distribution of ν_e event candidates including background contribution for a 5-year run with an assumption of $sin^2 2\theta_{13} = 0.10$, $sin^2 2\theta_{23} = 1.0$, and $\Delta m_{23}^2 = 0.003 eV^2$. The major background comes from the single π^0 NC production by ν_μ and from ν_e contamination in the beam. The analysis of this figure is summarized in
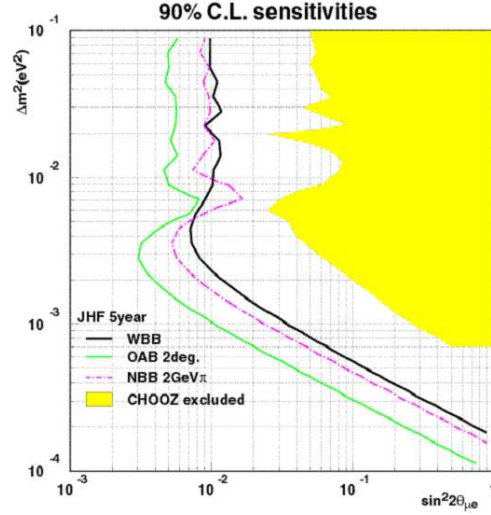
Figure 23: Sensitivities of JHFnu to Δm_{23} and $sin^2\theta_{\mu e}$.
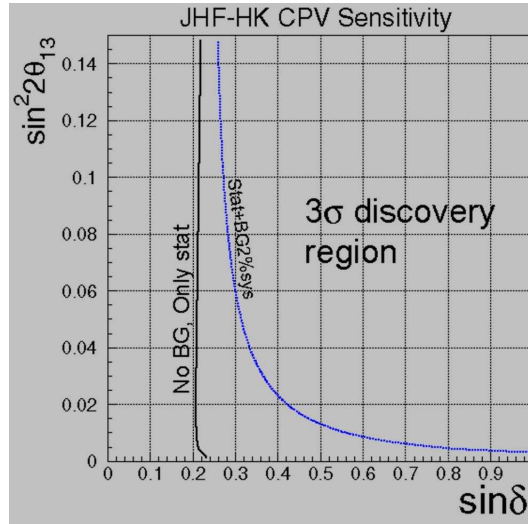
Figure 24: Sensitivity of upgraded JHFnu beam and Hyper-Kamiokande to sine of CP violating phase δ for given $sin^2 2\theta_{13}$.

Figure 23 where the sensitivity to $sin^2 2\theta_{13}$ is plotted indirectly in terms of $sin^2 2\theta_{\mu e}$ as a 90 % C.L. allowed region defined by the left-most (green) curve in the oscillation parameter space, Δm_{23}^2 vs $sin^2 2\theta_{\mu e}$ together with the CHOOZ excluded region (yellow shaded).

3.5 JHFnu and Hyper-Kamiokande

With a 1-Mton water Cherenkov detector, Hyper-Kamiokande and the upgraded JHFnu neutrino beam could lead to a much better sensitivity to $sin^2 2\theta_{13}$ as shown in Figure 24. Furthermore this second phase of JHFnu/Hyper-Kamiokande would be sensitive to CP
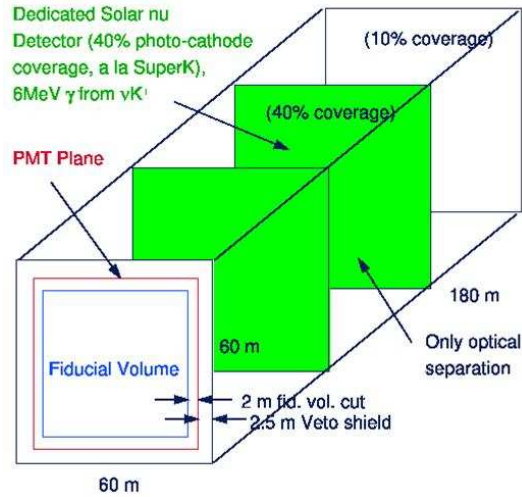
Figure 25: A sketch of the current UNO baseline detector.

violation in neutrino sector as also presented in this figure.

4. UNO

The goals of this project include searches for (or discovery of) nucleon decays, detection and detailed study of supernovas, and further detailed studies of atmospheric and solar neutrinos, searches for relic supernova neutrinos, and possibly detailed study of neutrino oscillation using a long baseline neutrino beam.

Whitepaper was written in July, 2002 which was signed by 49 members as a proto-collaborator and by 32 members as an interest group [6]. The proto-collaboration was upgraded to the collaboration in summer, 2003.

4.1 Detector

UNO is a next generation Underground Nucleon decay-neutrino Observatory which would use a much larger water Cherenkov detector than Super-Kamiokande. Figure 25 gives an idea of its structure and size. The current baseline design has 650 kton of water divided in three compartments which are optically but not physically isolated. The total physical size is $60 \times 60 \times 180 m^3$. Although the central compartment is equipped with photomultipliers (PMTs) that cover 40% of the surface, only 10 % of the surface of the two side compartments are covered with PMTs to reduce the cost without compromising the physics goals. The fiducial volume for nucleon decay searches and solar neutrino detection would be 440 ktons and 580 ktons for supernova or atmospheric neutrino detection.

4.2 Proton decay sensitivities

Figure 26 summarizes the sensitivities of a water Cherenkov detector to two important proton decays, $p \rightarrow e^+\pi^0$ and $p \rightarrow \nu K^+$ as a function of exposure time. It is assured that
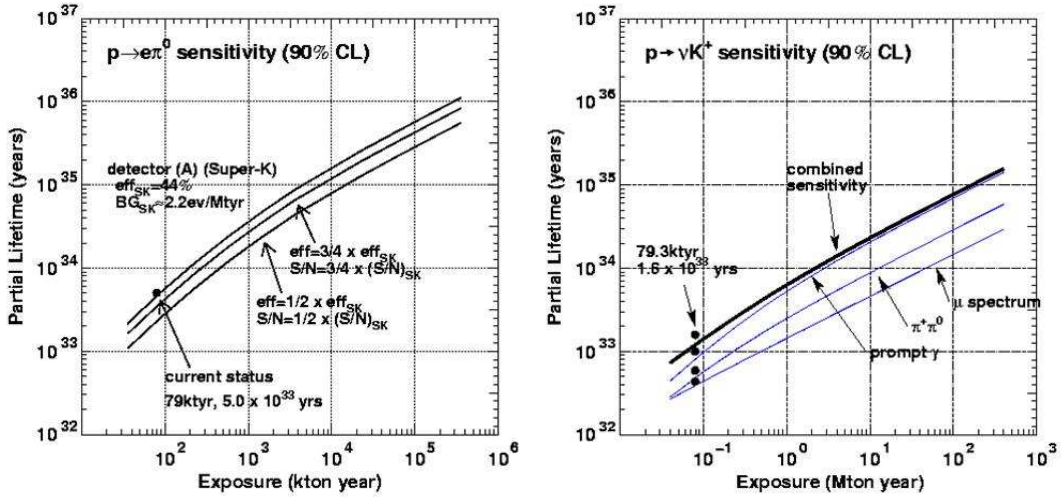
Figure 26: Left: Sensitivity to the proton decay $p \to e+\pi^0$ as a function of exposure time. Right: Sensitivity to the proton decay $p \to \nu K^+$ as a function of exposure time.
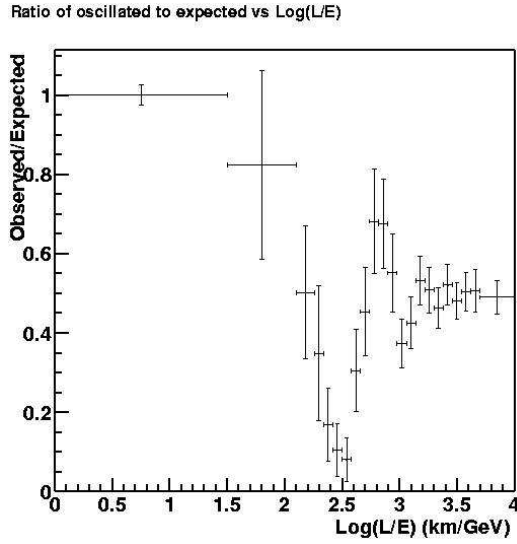
Figure 27: Oscillatory behavior of the L/E distribution of atmospheric neutrinos .

the current best limits on the partial proton lifetimes for these decay modes set by SK-I would be improved by a factor of 10.

4.3 Atmospheric neutrino oscillatory behavior

With a detector of UNO size it is possible to observe an oscillatory behavior in the L/E distribution of atmospheric neutrinos where L and E are the pathlength and energy of the neutrinos. This is clearly demonstrated in Figure 27 where an exposure time of 7 years is assumed together with the oscillation parameters of $sin^2\theta_{23} = 1$ and $\Delta m_{23}^2 = 0.003 eV^2$.
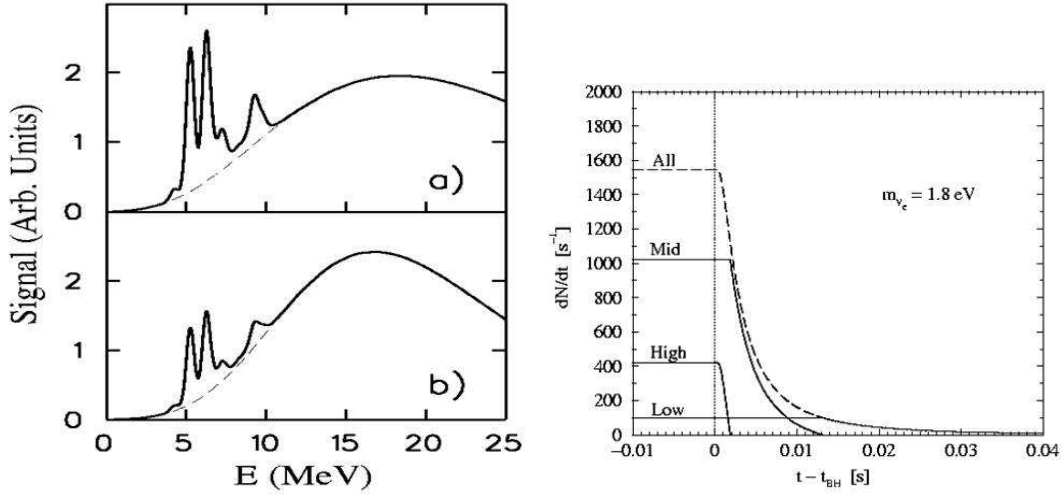
Figure 28: Left: Expected energy spectrum of supernova neutrinos 10 kpc away. Right: Expected supernova neutrino flux time profile when a black hole is created.

4.4 Supernova

Lastly if during the lifetime of UNO a supernova exploded as expected at the center of our Galaxy, 10 kpc away, UNO would detect 130,000 inverse beta decay events, 4,500 elastic scattering events and 4,500 neutral current (NC) events in the central compartment alone. Some of NC events that induce the transition $^{15}O \rightarrow ^{15}N$ could give very interesting information as shown in Figure 28 (left). Furthermore, if the protogenitor of the supernova were heavy enough, we could witness a birth of a black hole in real-time as illustrated in Figure 28 (right). When the black hole is formed, it is expected that the neutrino flux is suddenly and dramatically reduced as clearly shown in this figure.

References

[1] M. Honda et. al., *Phys. Rev.* **D 64** (2001) 53011

[2] J.N. Bahcall, M. H. Pinsonneault, S. Basu, *Astrophys. J.* **555** (2001) 990

[3] Q. R. Ahmad et. al., *Phys. Rev. Lett.* **89** (2002) 11301

[4] Brookhaven National Laboratory proposal: BNL-E889

[5] JHFnu Letter of Intent at http://neutrino.kek.jp/jhfnu

[6] UNO whitepaper at http://nngroup.physics.sunysb.edu